

# Improving the Intrinsic Properties of Mixed A-Cations Germanium Perovskite Solar Cells: Theoretical Prediction Using SCAPS 1-D

Mohd Saiful Adli Azizman,<sup>1,2</sup> Ayu Wazira Azhari,<sup>1,2\*</sup> Michelle Anak William,<sup>1,2</sup> Naimah Ibrahim,<sup>1,2</sup> Dewi Suriyani Che Halin,<sup>3,4</sup> Suhaila Sepeai,<sup>5</sup> Norasikin Ahmad Ludin<sup>5</sup> and Mohammad Nuzaihan Md Nor<sup>6</sup>

<sup>1</sup>Faculty of Civil Engineering and Technology, Universiti Malaysia Perlis, 02600 Jalan Kangar-Arau, Perlis, Malaysia

<sup>2</sup>Center of Excellence for Water Research and Environmental Sustainability Growth, Universiti Malaysia Perlis, 02600 Jalan Kangar-Arau, Perlis, Malaysia

<sup>3</sup>Faculty of Chemical Engineering and Technology, Universiti Malaysia Perlis, 02600 Jalan Kangar-Arau, Perlis, Malaysia

<sup>4</sup>Center of Excellence for Geopolymer & Green Technology, Universiti Malaysia Perlis, 02600 Jalan Kangar-Arau, Perlis, Malaysia

<sup>5</sup>Solar Energy Research Institute, Universiti Kebangsaan Malaysia, 43600 Bangi, Selangor, Malaysia

<sup>6</sup>Institute of Nano Electronic Engineering, Universiti Malaysia Perlis, 02600 Kangar, Perlis, Malaysia

\*Corresponding author: ayuwazira@unimap.edu.my

Published online: 28 November 2025

**To cite this article:** Azizman, M. S. A. et al. (2025). Improving the intrinsic properties of mixed A-cations germanium perovskite solar cells: Theoretical prediction using SCAPS 1-D. *J. Phys. Sci.*, 35(3), 55–74. https://doi.org/10.21315/jps2025.36.3.5

To link this article: https://doi.org/10.21315/jps2025.36.3.5

ABSTRACT: Compositional engineering technology has played a crucial role in the significant advancement of perovskite solar cells to produce high-quality and improved solar performance. Germanium is one of the potential replacements for the toxic lead active layer in perovskite solar cells due to its similar optical and electronic properties. However, germanium-based materials recorded the lowest efficiency of 8.6% compared to tin-based perovskites (< 13%) and lead-based materials (< 25%). To address this challenge, the influence of mixed A-cations (Methylammonium [MA], Formamidinium [FA], Ethylammonium [EA], Caesium [Cs]) with varied composition (0.25, 0.5, 0.75) on all possible combinations was investigated to estimate the structural and optoelectronic properties compatibility. This study used the SCAPS 1-D simulation tool to optimise the photoexcited charge carrier generation, collection and extraction. The findings show that a high doping concentration of caesium (> 50%) in germanium-based perovskite produced a perfect cubic-like structure with a tolerance factor ranging from 0.99 to 1.11. In addition, the optimum estimated bandgap for enhanced exciton generation was between 1.6 eV and 1.8 eV. Further optimisation revealed photovoltaic (PV) performance was optimised at an absorber thickness of 600 nm and maximum defect density of  $10^{16}$  cm<sup>-3</sup> (open-circuit voltage  $[V_{oc}] = 0.64$  V; short-circuit current density [J<sub>sc</sub>] = 16.55 mA/cm<sup>2</sup>; fill factor [FF] = 76.17% and power conversion efficiency (PCE) of 8.02%). The minimum carrier lifetime was calculated to be 10 ns

at a diffusion length of  $0.72~\mu m$  and further increased as the absorber quality improved. In addition, an optimal conduction band offset (CBO) range exists between -0.58~eV and -0.38~eV, with PCE above 10% and the materials with valence band offset (VBO) ranging from 0.67~eV to -0.23~eV will further improve the PV performance of mixed germanium-based perovskite solar cells. It is believed that this study can be helpful in developing and designing germanium-based solar cells for further improvement of the PV performance and increasing their potential to be a competitive material in lead-free variants.

Keywords: germanium, perovskite solar cells, mixed cations, SCAPS 1-D, lead free

### 1. INTRODUCTION

Perovskite solar cells (PSCs) have emerged as a promising technology due to their rapid efficiency gains and low manufacturing costs. However, the presence of lead (Pb) in these cells poses significant environmental and health concerns and has inspired research into Pb-free alternatives, including germanium (Ge)-based PSCs. The substitution of Pb with Ge in PSCs offers several potential advantages. Firstly, Ge is a less toxic element, reducing environmental risks associated with the manufacturing and disposal of these devices. Secondly, Ge may exhibit improved stability compared to Pb-based perovskites, particularly under long-term exposure to moisture and heat. This enhanced stability is crucial for the commercialisation and widespread adoption of PSCs. 3

One of the key factors influencing the performance and stability of PSCs is the composition of the A-cation site. Mixed A-cations, where multiple cations occupy the A-site of the ABX<sub>3</sub> structure, have shown significant promise in enhancing the properties of these materials. By introducing different cations, it is possible to tailor the crystal structure. Understanding the structural and electronic properties of mixed A-cations on Ge-based PSCs is crucial for optimising their performance and addressing the challenges associated with their development. Ge-based perovskites adopt a similar crystal structure to Pb-based perovskites, typically the cubic or tetragonal phase. This structural similarity allows for incorporating Ge into the perovskite lattice without significantly changing the overall material architecture. However, substituting Pb with Ge can lead to subtle differences in the lattice parameters, bond lengths, and electronic structure.<sup>4</sup>

Significant differences between Ge-based and Pb-based perovskites lie in their electronic properties. For instance, Ge has a smaller atomic radius compared to Pb (~0.77 Å, ~1.75 Å, respectively), which can influence the bandgap and charge carrier mobility. <sup>5,6</sup> Ge-based perovskites generally tend to have slightly wider bandgaps than their Pb-based counterparts. This wider bandgap can limit the absorption of sunlight in the visible spectrum, potentially reducing the overall efficiency of the solar

cell.<sup>7</sup> Moreover, the charge carrier mobility in Ge-based perovskites can be lower than in Pb-based perovskites, hindering the efficient collection of photogenerated carriers and leading to increased recombination losses and reduced device performance.<sup>8</sup> Additionally, the presence of Ge vacancies or defects will introduce energy levels within the bandgap, acting as recombination centres and further degrading the device's efficiency.

Despite these challenges, significant progress has been made in improving the performance of Ge-based PSCs, including exploring different Ge-based perovskite compositions to optimise the bandgap and charge carrier properties. The addition of organic cations such as methylammonium (MA), formamidinium (FA), or ethylammonium (EA) can help to improve the stability and phase purity of the perovskite layer while also allowing for tuning of the bandgap. Exploring different combinations and doping concentrations of inorganic and organic cations may enable optimal bandgaps and stability for Ge-based PSCs.

Furthermore, the quality of the absorber layer and the band offset at the interface between the absorber and charge-transporting layers play crucial roles in determining the performance of mixed A-cation Ge-based PSCs. <sup>11</sup> Device optimisation strategies are also crucial for improving the performance of mixed A-cation Ge-based PSCs. This includes optimising the perovskite layer's thickness and choosing suitable charge-transporting materials. The thickness of the absorber layer should be optimised to balance light absorption and charge carrier collection. A thicker absorber layer can improve light absorption but may also increase the distance that charge carriers need to travel to reach the electrodes, leading to increased recombination losses. <sup>12</sup> In addition, the band offset between the absorber layer and the charge-transporting layers is crucial for efficient charge carrier extraction.

A favourable band offset can promote the transfer of photogenerated holes to the hole transport layer (HTL) and electrons to the electron transport layer (ETL), minimising recombination losses. The interface between the absorber and charge-transporting layers can be engineered to improve charge carrier extraction. This can be achieved through interfacial layers or treatments that can modify the energy levels at the interface and reduce the barrier for charge carrier transfer. Thus, this study will provide the initial observation on material selection, optimising the absorber quality and interface layer band offset to further improve the photovoltaic (PV) properties of mixed A-cation Ge-based PSCs, making them a promising candidate for future renewable energy applications.

#### 2. MATERIALS AND METHODOLOGY

### 2.1 Prediction of Structural Stability and Bandgap

The structure stability of various mixed-cation Ge perovskite compositions is predicted using octahedra factor ( $\mu$ ) and Goldschmidt tolerance factor (t) for combinations of Cs, EA, FA and MA as the A-site cation as shown in Equation (1) and Equation (2), where  $r_A$  (EA, FA, MA),  $r_{A'}$  (Cs),  $r_B$  (Ge) and  $r_X$  (iodide [I]), respectively. Meanwhile, Equation (3) shows the mixed cations composition;  $r_{AA'}$ , with x = 0.25, 0.5 and 0.75. The effective ionic radii are used for 6 coordinate B-cation (Ge<sup>2+</sup>), considering the nature of the bond length of Ge to I halide ion; Ge-I as mentioned by Travis et al. On the other hand, the bandgap properties of proposed mixed perovskites are derived from undoped material using Vegard's law as shown in Equation (4), where  $E_g$  is energy gap in electron volt (eV).<sup>14</sup> The properties of respective ionic radii and undoped materials bandgap are tabulated in Table 1.

$$\mu = \frac{r_B}{r_X} \tag{1}$$

$$t = \frac{r_{AA'} + r_X}{\sqrt{2(r_{BB'} + r_X)}} \tag{2}$$

$$r_{AA'} = (x) r_A + (1 - x) r_{A'}$$
(3)

$$E_g(A_x A'_{1-x} B) = x E_g(AB) + (1-x) E_g(A'B)$$
 (4)

### 2.2 Simulation Procedures and Input Parameters

In this following study, the optimisation of optoelectronic properties for mixed A-cations Ge-based PSCs ( $A_xA'_{1-x}$ GeI<sub>3</sub>) is conducted based on the optimised active layer (AL) that may produce perovskite-like structure (0.81 < t < 1.1) with appropriate bandgap for solar cell application in n-i-p configuration of fluorine tin oxide; FTO/ETL/AL/HTL/ gold (Au), where titanium dioxide (TiO<sub>2</sub>) and  $C_{81}H_{68}N_4O_8$  (spiro-OMeTAD) are used as ETL and HTL using one-dimensional solar cell capacitance simulator (SCAPS 1-D) version 3.3.07 as illustrated in Figure 1 in illumination of AM1.5G, irradiance; 1000 w/m², temperature; 300 K, absorption interpolation;  $1 \times 10^5$  cm<sup>-1</sup> and AL defect density;  $10^{10}$  cm<sup>-3</sup>.15

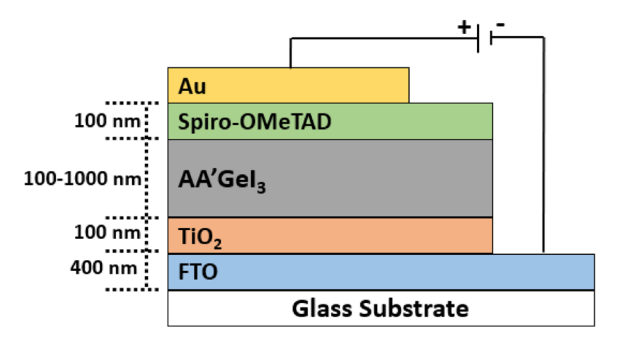


Figure 1: Configuration of studied cell structure.

This cell is further analysed in varied defect density ( $N_t = 10^{12} \, \text{cm}^{-3}$  to  $10^{20} \, \text{cm}^{-3}$ ) in terms of carrier diffusion length and absorber thickness (100 nm to 1000 nm) to maximise the photoexcited charge generation and collection in studied AL. Furthermore, the influence of varied conduction band offset (CBO) (0.02 eV to -0.98 eV) and valence band offset (VBO)( 0.67 eV to -0.33 eV) are analysed to improve the photoexcited charges extraction for ETL and HTL as given by Equation (5) and Equation (6), where  $\chi$  is electron affinity (eV) and  $E_g$  is band gap (eV). All input parameters are obtained from other published experimental and simulation studies and are tabulated in Table 2 to Table 4.

$$CBO(eV) = \chi_{AL} - \chi_{ETL \text{ or } HTL}$$
 (5)

$$VBO(eV) = (\chi_{AL} + Eg_{AL}) - (\chi_{ETL \text{ or HTL}} + Eg_{ETL \text{ or HTL}})$$
(6)

Table 1: Proposed mixed materials properties	able 1. Proposed	l mixed	materials	nroperties 5,16,	17
--	------------------	---------	-----------	------------------	----

Element	Ionic radii (Å)
Ge <sup>2+</sup>	0.77
FA <sup>+</sup>	2.53
$MA^{+}$	2.16
EA*	2.74
Cs <sup>+</sup>	1.88
I-	2.20
Perovskite	Bandgap (eV)
CsGeI <sub>3</sub>	1.60
$EAGeI_3$	1.30
FAGeI <sub>3</sub>	2.20
$MAGeI_3$	1.90

Table 2: Front and back contact parameters. 18

Parameter	n-	i-p
1 arameter	FTO	Au
Work function (eV)	4.4	5.1
Surface recombination velocity of electrons (cm/s)	$1 \times 10^5$	$1\times10^7$
Surface recombination velocity of holes (cm/s)	$1\times10^7$	$1 \times 10^5$

Table 3: Interlayer defect parameters.<sup>19</sup>

Parameter	Perovskite/ETL	HTL/Perovskite	
Defect type	Neutral		
Capture cross-section of electrons and holes (cm <sup>-2</sup> )	$1 \times 10^{-15}$		
Energetic distribution	Single		
Energy with respect to reference	0.6 eV above highest Ev		
Integrated total density (cm <sup>-3</sup> )	1 ×	$10^{15}$	

Table 4: Conductive and electron transport layer properties. 16,18,20

	TCO	ETL	Al	L	HTL
Parameter	FTO	TiO <sub>2</sub>	MA-based	Cs-based	Spiro- OMeTAD
Thickness (μm)	0.4	0.1	0.1 to	1.0	0.1
Bandgap (eV)	3.4	3.26	This s	tudy	3.26
Electron affinity (eV)	4.4	4.2	3.98	3.52	4.2
Relative dielectric permittivity (dimensionless)	9	10	10	10	10
Conductive band density of state (cm <sup>-3</sup> )	$2.2\times10^{18}$	$2.2\times10^{18}$	$1\times10^{16}$	$1\times10^{18}$	$2.2\times10^{18}$
Valence band density of state (cm <sup>-3</sup> )	$1.8\times10^{19}$	$1.8\times10^{18}$	$1\times10^{15}$	$1\times10^{19}$	$1.8\times10^{18}$
Electron thermal velocity (cm/s)			$1\times 10^7$		
Hole's thermal velocity (cm/s)			$1\times 10^7$		
Electron's mobility (cm²/Vs)	20	100	16.2	20	100
Holes mobility (cm <sup>2</sup> /Vs)	10	25	10.1	20	25
Donor concentration (cm <sup>-3</sup> )	$2\times10^{19}$	$1\times10^{19}$	$1 \times 10^9$	0	$1\times10^{19}$
Acceptor concentration (cm <sup>-3</sup> )		0	$1 \times 10^9$	$2\times10^{16}$	0
Defect density (cm <sup>-3</sup> )	1 ×	$10^{15}$	$1 \times 10^{10} \text{ to}$	$1 \times 10^{20}$	$1 \times 10^{15}$

#### 3. RESULTS AND DISCUSSION

### 3.1 Structural Stability

The structural stability of ABX<sub>3</sub> active materials is empirically predicted using the Goldschmidt tolerance factor (t) and has been very successful in describing other perovskite materials (e.g.,  $Pb^{2+}$ ,  $Sn^{2+}$ ). In this study, the majority of proposed Ge-based active materials (13 out of 18) are structurally stable with t ranging from 0.99 to 1.11 and MACs with a higher doping concentration of Cs (> 50%) has perfect cubic-like perovskite structure as shown in Figure 2. Meanwhile, other mixed materials may produce a non-perovskite structure due to larger A-cation and cannot be fitted into ABX<sub>3</sub> crystal with t > 1.11. On the other hand, the octahedral factor ( $\mu$ ) is calculated to be 0.35 for all materials and significantly lower than the stability limit of the BX<sub>6</sub> octahedron (0.4 <  $\mu$  < 0.9). Interestingly, due to the stereo-chemical active lone pair phenomenon, the crystal structure stability requirement (t and  $\mu$ ) may not be applicable for Ge-based perovskite. This exclusion is specifically for group 14 elements because stereo-chemical active lone pairs in the 2+ state are only available in this variant.<sup>21</sup>

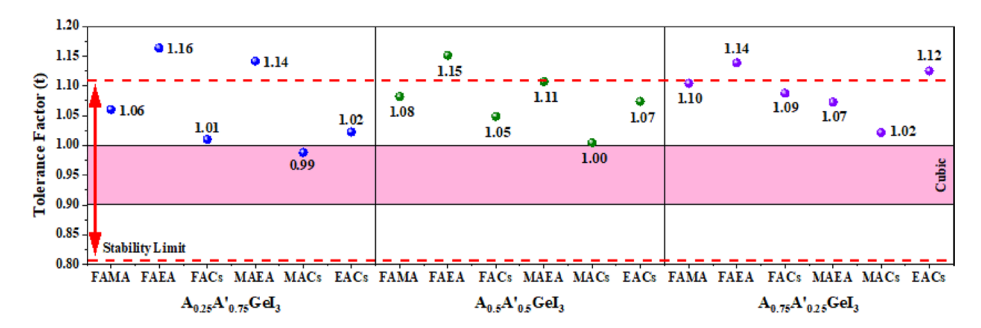


Figure 2: Predicted tolerance factor.

The perovskite structure formation of mono-cation Ge-based materials was confirmed by Stoumpos et al. in 2015.<sup>22</sup> The reported octahedra (BX<sub>6</sub>) properties of the germanium-iodide (Ge-I) have revealed that this structure is stable and generated from the trigonal pyramidal units wrapped around the A-cation spacers. The synthesised active materials are categorised as R3m, P2<sub>1</sub>, P2<sub>1</sub>/c, P6<sub>3</sub> and I-42d space groups depending on the degree of distortion, orientation axis and size of A-cation-iodide cuboctahedra (AX<sub>12</sub>). Moreover, the Ge-based compounds also display highly distorted GeI<sub>6</sub> octahedra with 3 longer and 3 shorter Ge–I bond in CsGeI<sub>3</sub>, FAGeI<sub>3</sub> and MAGeI<sub>3</sub>, indicating the intrinsic stereo-chemical active lone pair characteristics of Ge<sup>2+</sup>, which have led to the structural adaptation while maintaining the stable AGeI<sub>3</sub> perovskite-like structure.<sup>22</sup>

On the other hand, Yue et al. also successfully synthesised mixed cations Ge-based active materials in 2019 using FA-MA in varied concentrations (0.25 to 0.75).9 The XRD analysis has confirmed that the crystal structure of mixed compounds features a similar profile shape to their parent compounds.9 Therefore, the proposed mixed A-cations in this study are expected to have similar BX<sub>6</sub> and AX<sub>12</sub> adaptations. Nevertheless, as part of preliminary material screening in optimising mixed cations Ge-based PSCs, any materials with a tolerance factor of 0.81 to 1.11 are selected for bandgap prediction.

# 3.2 Calculated Bandgap

The calculated bandgap of active materials that surpassed the tolerance factor requirement is denoted from 1 to 13 and tabulated in Table 5. Estimated bandgaps are considered acceptable with less than 3% margin error compared to synthesised mixed materials;  $FA_xMA_{1-x}GeI_3$  (x = 0.25, 0.5 and 0.75) by Yue et al.<sup>9</sup> Among all 13 predicted bandgaps, only 3 mixed Ge-based materials (sample no. 4, 7, 9) have narrow bandgap ( $\leq$  1.60 eV). In contrast, other materials have a wider bandgap of more than 1.60 eV. The semiconducting materials with lower bandgaps are essential for capturing more visible solar spectrum and have been utilised in high-performing PSCs (1.40 eV to 1.60 eV).<sup>23,24</sup>

The bandgap is the energy difference between the conduction band minimum and valence band maximum and directly influences optoelectronic characteristics. The ability to modify the bandgap has made PSCs appealing for various applications (e.g., PVs, light-emitting devices and particle detection).<sup>25</sup> Theoretically, the A-site cation plays an indirect role in the band structure by influencing the bond lengths, bandgap and B-X angles, either through octahedral tilting of sub-lattice or steric interactions.<sup>26</sup> In mono and mixed cations of Ge-based PSCs incorporating Cs, FA and MA, the bandgap increases with increasing the size of the A-cation (Cs < MA < FA) due to the incremental of spatial separation of the GeI<sub>3</sub> units and weaker orbital overlap, resulting narrow bandwidths and larger band separation. 9,22 On the contrary, EA cations (2.74 Å) have larger unit cells than Cs, MA and FA. Thus, the Ge-I bond will be longer. Since the energy bandgap in perovskites is attributed to the valance and conduction band formed by Ge-4p, Ge-4s and I-4p orbitals overlapping, Ge-I bond interaction with I-5p and Ge-5p orbital will be lesser as compared to smaller unit cells (e.g., MAGeI<sub>3</sub>).<sup>17</sup> Therefore, the bandgap of perovskite materials utilising EA is expected to be less than mixed materials.

Table 5: Estimated mixed cations bandgap.

	$A_xA$	' <sub>1-x</sub> GeI <sub>3</sub>		Estimated bandgap, Eg; Experimental bandgap <sup>9</sup>		Estimated bandgap, Lg,						
A	A'	X	1-x	eV/ (sample no.)	Active material	E <sub>g</sub> (eV)	%					
FA	MA			1.98 (1)								
FA	Cs	0.25	0.75	1.75 (2)	E4 144 C.I	2.02	2.71					
MA	Cs	0.25	0./5	0.75 $1.68 (3)$ $FA_{0.25}MA_0$	$FA_{0.25}MA_{0.75}GeI_3$	2.03	2.71					
EA	Cs			1.53 (4)								
FA	MA			2.05 (5)								
FA	Cs			1.90 (6)								
MA	EA	0.50	0.50	0.50	0.50	0.50	0.50	50 0.50	1.60 (7)	$FA_{0.50}MA_{0.50}GeI_3$	2.10	2.38
MA	Cs			1.75 (8)								
EA	Cs			1.45 (9)								
FA	MA			2.13 (10)								
FA	Cs	0.75	0.25	2.05 (11)	FA <sub>0.75</sub> MA <sub>0.25</sub> GeI <sub>3</sub>	2.19	2.97					
MA	EA		0.29	1.75 (12)	1110./5111110.25 (1013	2.17	2.77					
MA	Cs			1.83 (13)								

### 3.3 Optimising Optoelectronic Properties

The preliminary screening of suitable active materials for Ge-based PSCs is analysed in n-i-p planar structure of FTO/TiO<sub>2</sub>/AL/Spiro-OMeTAD/Au with batch simulation of different bandgap ranging from 1.0 eV to 2.0 eV. Since the majority of mixed materials that surpassed the tolerance factor contained MA (sample no. 1, 5, 7, 10, 12, 13) or Cs (2-4, 6, 9, 11) as main and doping cation with higher concentration, the PV properties are compared using two sets of AL properties as shown in Figure 3 except for sample no. 8 (equivalent concentration of MA and Cs) was then compared with both properties. In MA-based materials, the highest power conversion efficiency (PCE) (> 10%) could potentially be achieved by tailoring the bandgap between 1.0 eV to 1.2 eV. Unfortunately, as the J<sub>sc</sub>, FF and PCE continuously to decreased as the bandgap become wider, no proposed mixed materials fall within the optimal region. The narrowest bandgap is only observed in MA<sub>0.5</sub>EA<sub>0.5</sub>GeI<sub>3</sub>; sample no. 7 with  $E_g$  of 1.60 eV and PCE at 5.78% ( $V_{oc}$ ; 0.88 V,  $J_{sc}$ ; 9.64 mA/cm<sup>2</sup>, FF; 68.14%). On contrary, the PV characteristics for Cs-based cell is vigorously soared up as the bandgap increased. The maximum performance in range of 1.6 eV < Eg < 1.8 eV may possibly be obtained on sample no. 2 and 8 (FA<sub>0.25</sub>Cs<sub>0.75</sub>GeI<sub>3</sub>, MA<sub>0.5</sub>Cs<sub>0.5</sub>GeI<sub>3</sub>) with similar  $E_g$  at 1.75 eV and  $V_{oc}$  recorded at 0.61 V,  $J_{sc}$ ; 7.47 mA/cm<sup>2</sup>, FF; 76.38%. Nevertheless, the PCE is relatively lower (3.46%) compared to MA<sub>0.5</sub>EA<sub>0.5</sub>GeI<sub>3</sub>.

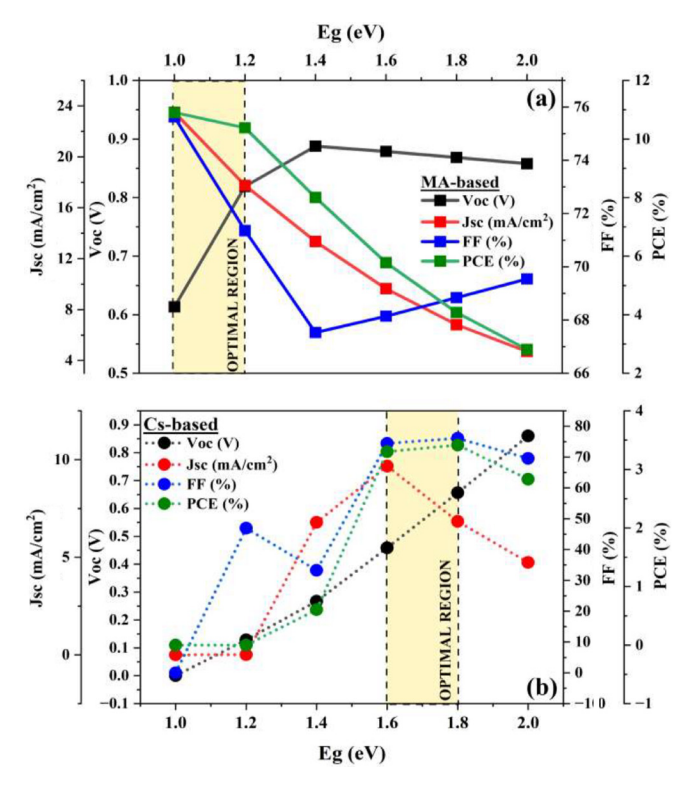


Figure 3: PV performance in varied bandgap; (a) MA-based and (b) Cs-based

The optimal bandgap range of 1.6 eV to 1.8 eV is crucial for maximising the PV properties of Ge-based PSCs, primarily through its impact on light absorption. Specifically, a bandgap within this range allows for efficient absorption of photons with energies equal to or greater than the bandgap and directly translates to a higher photocurrent ( $J_{sc}$ ). The observed PV properties in Cs-based materials indicated that a lower bandgap (less than 1.6 eV) leads to excess energy, where a large number of lower energy photons are absorbed and lost through thermalisation losses, affecting the  $V_{oc}$ . Moreover, a bandgap greater than 1.8 eV suggests fewer photons are absorbed, leading to a low  $J_{sc}$ . Therefore, the 1.6 eV to 1.8 eV range represents a balance where a substantial portion of the solar spectrum is absorbed, contributing to a high  $J_{sc}$ , while maintaining a reasonable  $V_{oc}$ .

Furthermore, a bandgap within the 1.6 eV to 1.8 eV range that is well-matched ensures that enough electron-hole pairs are generated to create a high  $J_{sc}$  and indirectly indicates an enhanced absorption spectrum to the solar irradiance spectrum. <sup>28</sup> On the other hand, the theoretical potential for MA-based materials with a bandgap of 1.0 eV to 1.2 eV range is promising; however, the observed PV properties show a decrease in  $J_{sc}$ , FF and PCE with wider bandgaps, suggesting that the quality of

absorption and charge carrier dynamics is not optimised. The absorption of photons is still occurring beyond 1.2 eV, but the charge carriers created quickly recombine, resulting in a low  $J_{sc}$ . These results suggest that while bandgap engineering is crucial, optimising material quality and charge carrier dynamics is equally important for achieving high-performance solar cells.<sup>29</sup>

The A-site cation in ABX $_3$  perovskites plays a crucial role in determining the overall crystal structure and symmetry. It is often considered that A-site atoms have a lesser impact on the band structure compared to B-site and X-site atoms. However, they can still significantly influence the material's properties, particularly stability. Research led by Saliba et al. has demonstrated the effectiveness of using mixed A-site cations to enhance the performance of PSCs. By introducing a mixture of Rb, Cs, MA and FA cations at the A-site within the APbI $_3$  structure, they achieved a remarkable PCE of 21.6% with a  $V_{oc}$  of 1.24 V and a bandgap of 1.62 eV. The mixed-cation approach can improve the stability of perovskite materials, as demonstrated by the 95% retention of initial performance after 500 h of ageing under steady air mass (AM) 1.5G illumination at 85°C in a nitrogen environment proved the mixing A-site cations can allow for fine-tuning of the material's properties, such as bandgap and crystal structure.<sup>30</sup> This can be beneficial for tailoring perovskites for specific applications as the development of cost-effective solar cells requires both optimised fabrication techniques and efficient PV design.<sup>31</sup>

### 3.4 Optimising Photoexcited Charge Generation and Collection

The optimisation of charge carrier generation and collection as a measure of absorber quality is evaluated in varied defect density ( $N_t = 10^{12}$  to  $10^{20}$  cm<sup>-3</sup>) in terms of AL thickness (200 nm to 1000 nm) as shown in Table 6 for Cs-based absorber (FA<sub>0.25</sub>Cs<sub>0.75</sub>GeI<sub>3</sub> and MA<sub>0.5</sub>Cs<sub>0.5</sub>GeI<sub>3</sub>) with estimated bandgap of 1.75 eV. The correlation of carrier lifetime ( $\tau$ ) and diffusion length (*LD*) are given by Equation (7), where D is diffusion coefficient.

$$L_D = (D\tau)^{1/2} \tag{7}$$

**Table 6:** Carrier diffusion length and carrier lifetime in term of defect density.

Defect density, N <sub>t</sub> (cm <sup>-3</sup> )	1012	$10^{14}$	1016	$10^{18}$	$10^{20}$
Diffusion length, $L_D$ ( $\mu$ m)	72	7.2	0.72	0.072	0.0072
Carrier lifetime, $\tau$ (ns)	$10^{5}$	$10^{3}$	10	$10^{-1}$	$10^{-3}$

Figure 4 (a) illustrated the PCE performance along with  $L_D$  as a function of absorber thickness. The wide absorbers (< 600 nm) with improved absorber quality;  $N_t < 10^{16} \text{ cm}^{-3}$  and  $L_D$  more than 0.72  $\mu m$ , able to maintain a PCE above 8%.

A significant increase in  $J_{sc}$  was also observed due to lower defect density and lesser recombination of carriers. However, shorter diffusion length as the defect density increased compromises the  $J_{sc}$ .  $^{32}$  Recorded  $J_{sc}$  across all studied thickness revealed that  $L_D=0.0072~\mu m~(N_t;~10^{20}~cm^{-3})$ , has the lowest  $J_{sc}$  ranging from 2.84 mA/cm² at 200 nm and 2.60 mA/cm² at 1,000 nm as shown in Figure 4 (b). The  $J_{sc}$  only improved by more than 11 mA/cm² once the  $L_D$  was at 0.072  $\mu m$  and above. Recombination is strongly dependent on both  $\tau$  and  $L_D$ , while the recombination rate depends on defects in the material. As  $N_t$  increases from  $10^{12}~cm^{-3}$  to  $10^{20}~cm^{-3}$ , the recombination increases near the junction resulting a loss in  $V_{oc}$  due to decreases in  $L_D$  as shown in Figure 4 (c) and the majority of free-flow electrons through the solar cell contributing to the high generation of a photon to electron as the  $L_D$  is increased, and consequently, the  $J_{sc}$  will rise. On the other hand, if the generated carrier is closer to the surface, it is likely to recombine due to low  $L_D$  and result in a low  $J_{sc}$ .

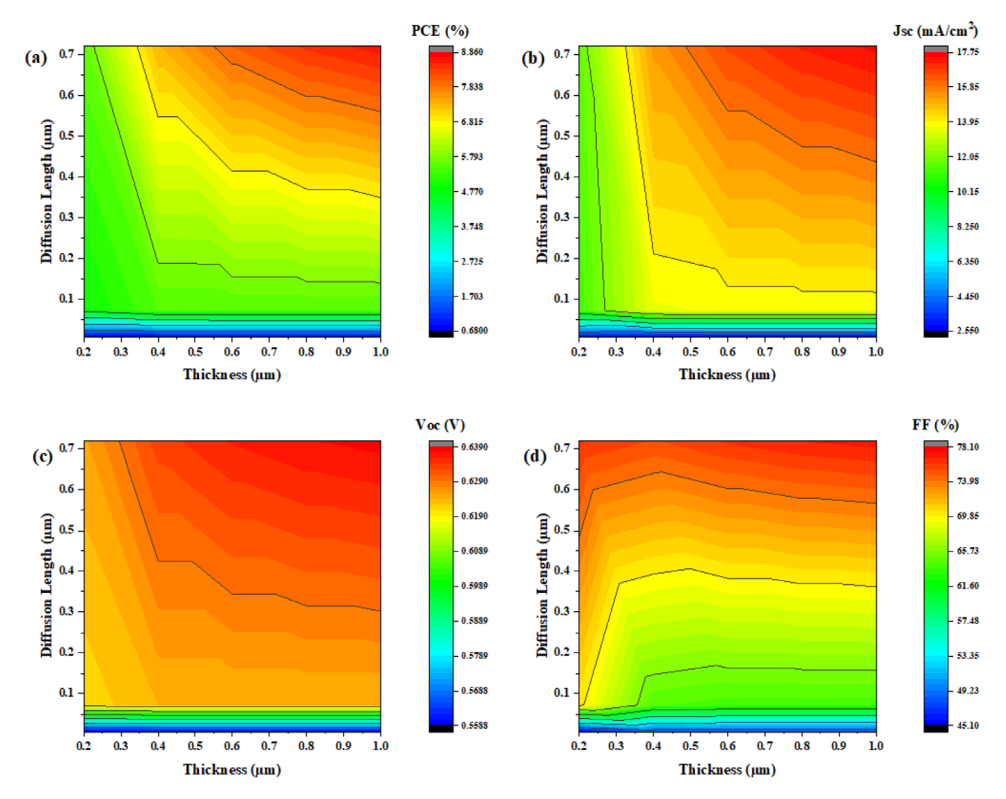


**Figure 4:** PV performance in terms of diffusion length at  $0.0072 \,\mu m$  to  $0.72 \,\mu m$  and absorber thickness; (a) PCE, (b)  $J_{sc}$ , (c)  $V_{oc}$  and (d) FF.

Among all studied PV parameters, the FF is the most critical factor that will influence the cell performance, as the electric field delivered to the absorber is reduced as the forward bias increases, hence collecting a more significant number of carriers. At 600 nm thickness, the FF rose from 47.98% ( $L_D = 0.0072~\mu m$ ) to 76.63% ( $L_D = 72~\mu m$ ) due to improved quality of the absorber layer as the  $N_t$  decreased from  $10^{20}~cm^{-3}$  to  $10^{12}~cm^{-3}$ . Similar behaviour was also recorded for all studied AL thicknesses with the FF as low as 45.15% (200 nm) at  $L_D$  of 0.0072  $\mu m$  to the highest FF at 78.02% ( $L_D = 72~\mu m$ ), 1000 nm as shown in Figure 4 (d). The optimum performance of  $FA_{0.25}Cs_{0.75}GeI_3$  and  $MA_{0.5}Cs_{0.5}GeI_3$  PSCs as ALs for Gebased PSCs, which potentially improve PV performance, is selected at an absorber thickness of 600 nm with a maximum  $N_t$  of  $10^{16}~cm^{-3}$ , considering the impact of defect density and absorber layer thickness. The minimum carrier lifetime under AM1.5G illumination is calculated to be 10 ns ( $N_t = 10^{16}~cm^{-3}$ ) and will further increase as the absorber quality improves with  $V_{oc}$  at 0.64 V,  $J_{sc}$ ; 16.55 mA/cm², FF; 76.17% and PCE of 8.02%.

## 3.5 Optimising Charge Carrier Extraction

#### 3.5.1 Performance in varied CBO

The performance of a PSC is primarily determined by the ability to generate and extract charge carriers effectively. Charge carrier extraction involves the process of collecting and transporting generated electrons and holes to the external circuit. This process is crucial for maximising the power output of the cell.<sup>35</sup> Intrinsically, the Gebased active materials act as a p-type absorber, and electrons are the minority carrier.<sup>36</sup> Therefore, the magnitude of band offset (CBO and VBO) between AL and charge extracting layers is important. These offsets represent the energy difference between the conduction band (CB) or valence band (VB) of the absorber layer and the adjacent layers (e.g., electron and hole transport layers).<sup>37</sup> The simulation results highlight the critical role of CBO in optimising device performance as tabulated in Table 7 with CBO values at ranging from 0.02 eV to –0.98 eV. A positive CBO, often referred to as a spike heterojunction, create an energy barrier for electron injection from the perovskite layer to the electron transport layer. This barrier can hinder charge carrier extraction, leading to reduced power output and efficiency.<sup>38</sup>

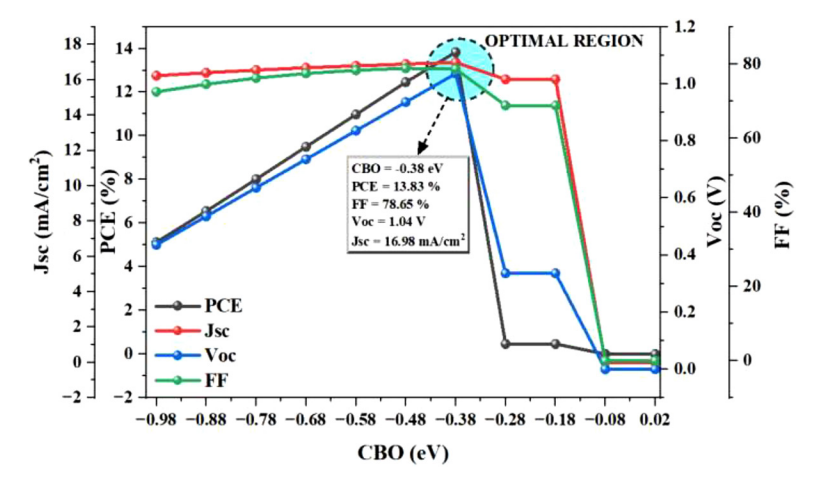


Figure 5: Cell performance in varied conduction band offset

On the other hand, a negative CBO, known as a cliff band offset, creates a potential well for electrons in the perovskite layer. While a moderate negative CBO can enhance electron injection and reduce recombination losses, an excessively negative CBO can lead to increased electron trapping and degraded performance.<sup>39</sup> The results suggest that an optimal CBO range exists between -0.58 eV and -0.38 eV with PCE above 10%. Within this range, the CBO creates a suitable energy barrier for electron injection while minimising electron trapping, resulting in improved PCE,  $J_{sc}$ ,  $V_{oc}$  and FF. However, deviating from this optimal CBO range can have adverse effects. A CBO that is too positive ( $\leq 0.02$  eV) and a minimal negative CBO (-0.08 eV) can create an excessive energy barrier for electron injection, while a CBO that is too negative (below -0.38 eV) can lead to increased electron trapping, as shown in Figure 5.

Tal	ole 7: [	Гуре о	f cond	luction	band	and	PV	performance.
-----	----------	--------	--------	---------	------	-----	----	--------------

CBO (eV)	Туре	PCE (%)	J <sub>sc</sub> (mA/cm <sup>2</sup> )	V <sub>oc</sub> (V)	FF (%)
0.0200	spike	0.0000	0.0000	0.0000	0.0000
-0.0800	cliff	0.0000	0.0000	0.0000	0.0000
-0.1800	cliff	0.4631	16.0287	0.3358	68.7773
-0.2800	cliff	0.4631	16.0287	0.3358	68.7773
-0.3800	cliff	13.8340	16.9768	1.0360	78.6544
-0.4800	cliff	12.4586	16.8918	0.9358	78.8129
-0.5800	cliff	10.9803	16.7892	0.8358	78.2478
-0.6800	cliff	9.4992	16.6798	0.7358	77.4256
-0.7800	cliff	8.0151	16.5496	0.6358	76.1698
-0.8800	cliff	6.5495	16.4014	0.5358	74.5244
-0.9800	cliff	5.1260	16.2303	0.4358	72.4653

#### 3.5.2 Performance in varied VBO

A favourable VBO at the perovskite/HTL interface can facilitate efficient hole extraction from the perovskite layer, leading to improved  $V_{oc}$  and FF due to favourable mobility of holes from the perovskite to the HTL, reducing recombination losses and enhancing the overall PCE of the solar cell as estimated in Table 8. Conversely, a mismatch in VBO can have significant implications for the performance of PSCs including reduced hole extraction; create an energy barrier for hole extraction, hindering the movement of holes from the perovskite layer to the HTL, increased recombination; VBO mismatch can also introduce interfacial defects or states that act as recombination centres, leading to increased recombination losses and energy level misalignment; disrupt the energy level alignment between the perovskite and HTL, affecting the overall charge carrier dynamics and device performance.<sup>40</sup> The VBO for Cs-based absorber and HTL has a broader selection of materials ranging from 0.67 eV to -0.23 eV, with optimum performance recorded at VBO of -0.03 eV (PCE: 8.26%,  $J_{sc}$ : 16.92 mA/cm<sup>2</sup>,  $V_{oc}$ : 0.64 V, FF: 71.07%). As seen from the optimisation of CBO and VBO, both FA<sub>0.25</sub>Cs<sub>0.75</sub>GeI<sub>3</sub> and MA<sub>0.5</sub>Cs<sub>0.5</sub>GeI<sub>3</sub> ALs with a bandgap of 1.75 eV, the electrons flow in these cells are more favourable in cliff band type compared to holes, which is more suitable in spike band offset with no drastic drop in performance.

The lowest performance was observed at a VBO of -0.33 eV, with a PCE of 0.29%,  $J_{sc}$  of 1.97 mA/cm<sup>2</sup>, a  $V_{oc}$  of 0.6366 V and an FF of 22.92%. As the VBO becomes more positive, the PV performance gradually decreases. This suggests that a more positive VBO creates an energy barrier for hole extraction, hindering the movement of charge carriers from the perovskite layer to the hole transport layer.<sup>41</sup> However, as the VBO becomes more negative, the trend is more complex. While the PCE continues to decrease, the  $V_{\text{oc}}$  remains relatively stable at around 0.63 V. The J<sub>sc</sub> increases significantly, reaching a maximum of 17 mA/cm<sup>2</sup> at a VBO of -0.23 eV. The FF also remains relatively high, above 63%, until the VBO reaches -0.23 eV. Beyond -0.23 eV, both J<sub>sc</sub> and FF begin to decrease rapidly. At VBO values of -0.23 eV and -0.33 eV, the J<sub>sc</sub> drops to 1.97 mA/cm<sup>2</sup> and the FF decreases to 51% and 22.9%, respectively, as illustrated in Figure 6. These results suggest that there exists an optimal VBO range for the studied mixed A-cations of Ge-based PSCs. A VBO that is too positive can create an energy barrier for hole extraction, while a VBO that is too negative can lead to increased electron trapping and reduced device performance, proving that identifying and optimising the optimal VBO in absorber/HTL material and device architecture is crucial for achieving high efficiency PSCs. 42,43

VBO (eV)	Type	PCE (%)	J <sub>sc</sub> (mA/cm <sup>2</sup> )	$V_{oc}(V)$	FF (%)
	7.1		,		
0.6700	spike	4.1746	15.0684	0.4360	63.5398
0.5700	spike	5.4775	15.2890	0.5354	66.9129
0.4700	spike	6.7561	15.4808	0.6164	70.8002
0.3700	spike	7.4021	15.6691	0.6331	74.6228
0.2700	spike	7.5763	15.8865	0.6341	75.2069
0.1700	spike	7.7563	16.1625	0.6348	75.5942
0.0700	spike	8.0151	16.5496	0.6358	76.1698
-0.0300	cliff	8.2563	16.9233	0.6370	76.5927
-0.1300	cliff	7.7391	17.0751	0.6377	71.0708
-0.2300	cliff	5.6053	17.0405	0.6374	51.6029
-0.3300	cliff	0.2874	1.9694	0.6366	22.9232

**Table 8:** Type of valence band and corresponding performance.

Both CBO and VBO play crucial roles in determining the performance of PSCs. Optimising these parameters is essential for achieving high efficiency and stability. A moderate negative CBO is generally beneficial for electron injection and device performance. However, an excessively negative CBO can lead to increased electron trapping and reduced efficiency. Meanwhile, favourable VBO is essential for efficient hole extraction and overall device performance, as a mismatch in VBO can introduce energy barriers and recombination losses. The interplay between CBO and VBO is complex and can significantly impact device performance. Optimising both parameters is crucial for achieving the best results. 44,45

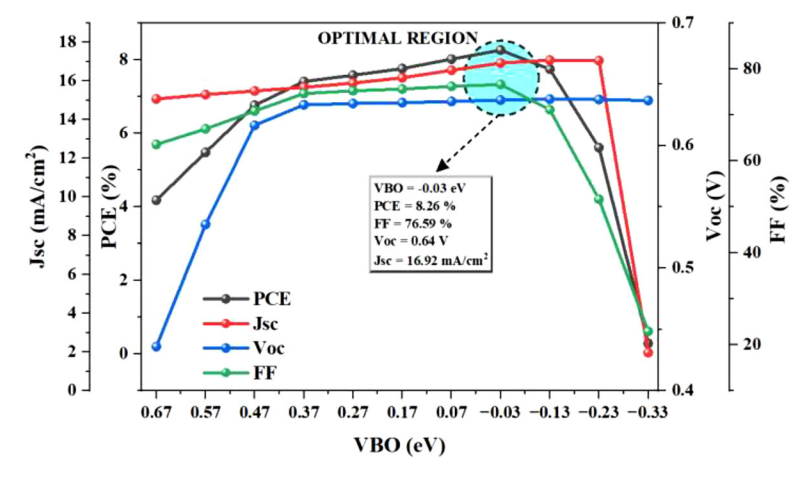


Figure 6: Cell performance in varied valence band offset.

#### 4. CONCLUSION

This study has investigated the impact of mixed A-cations on the intrinsic properties of Ge-based PSCs. By systematically exploring different A-cation compositions and employing simulation techniques, we have identified key factors that influence device performance. Our findings demonstrate the significant potential of mixed A-cations in enhancing the PV properties of Ge-based PSCs. By optimising the mixed A-cation composition, we have achieved a promising combination that leads to a perfect cubic-like crystal structure, a desirable bandgap, and reduced defect density.

Furthermore, our simulations have revealed the importance of device optimisation. An absorber thickness of 600 nm and a defect density less than  $10^{16}$  cm<sup>-3</sup> have been identified as optimal for maximising power conversion efficiency. The calculated carrier lifetime of 10 ns indicates the potential for further improvements through enhanced absorber quality. In addition to optimising the intrinsic properties of the perovskite material, careful consideration of the interfaces between the perovskite layer and the charge-transport layers is essential. Moreover, suitable ETL and HTL materials within the proposed CBO and VBO may improve the charge carrier extraction and transport, leading to higher cell performance. Overall, this study highlights the promising potential of mixed A-cation Ge-based PSCs. Thus, pave the way for the development of high efficiency and stable solar cells that contribute to a sustainable energy future.

### 5. ACKNOWLEDGEMENTS

The authors would like to acknowledge the support from the Fundamental Research Grant Scheme under grant number FRGS/1/2021/TK0/UNIMAP/02/49 from the Ministry of Higher Education Malaysia.

#### 6. REFERENCES

- 1. Bati, A. S. R. et al. (2023). Next-generation applications for integrated perovskite solar cells. *Commun. Mater.*, 4, 2. https://doi.org/10.1038/s43246-022-00325-4
- Magdalin, A. E. et al. (2023). Development of lead-free perovskite solar cells: Opportunities, challenges, and future technologies. *Res. Eng.*, 20, 101438. https://doi.org/10.1016/j.rineng.2023.101438
- 3. Liu, J. et al. (2023). Optimizing the performance of Ge-based perovskite solar cells by doping CsGeI3 instead of charge transport layer. *Sol. Energy*, 259, 398–415. https://doi.org/10.1016/j.solener.2023.04.002
- 4. Chiara, R. et al. (2021). Germanium-based halide perovskites: Materials, properties, and applications. *Chempluschem.*, 86(6), 879–888. https://doi.org/10.1002/cplu.202100191

- 5. Travis, W. et al. (2016). On the application of the tolerance factor to inorganic and hybrid halide perovskites: A revised system. *Chem. Sci.*, 7, 4548–4556. https://doi.org/10.1039/C5SC04845A
- 6. Sulaymon, A. H. et al. (2013). Competitive biosorption of lead, cadmium, copper, and arsenic ions using algae. *Environ. Sci. and Pollut. Res.*, 20, 3011–3023. https://doi.org/10.1007/s11356-012-1208-2
- 7. Islam, J. & Hossain, A. K. M. A. (2020). Narrowing band gap and enhanced visible-light absorption of metal-doped non-toxic CsSnCl<sub>3</sub> metal halides for potential optoelectronic applications. *RSC Adv.*, 13, 7817–7827. https://doi.org/10.1039/C9RA10407K
- 8. Herz, L. M. (2017). Charge-carrier mobilities in metal halide perovskites: Fundamental mechanisms and limits. *ACS Energy Lett.*, 2(7), 1539–1548. https://doi.org/10.1021/acsenergylett.7b00276
- 9. Yue, S. et al. (2019). Synthesis, characterization, and stability studies of Ge-based perovskites of controllable mixed cation composition, produced with an ambient surfactant-free approach. *ACS Omega*, 4, 18219–18233. https://doi.org/10.1021/acsomega.9b02203
- 10. Ribeiro, I. C. et al. (2024). Unveiling the impact of organic cation passivation on structural and optoelectronic properties of two-dimensional perovskites thin films. *Appl. Surf. Sci.*, 678, 161098. https://doi.org/10.1016/j.apsusc.2024.161098
- 11. Córdoba, M. & Taretto, K. (2024). Insight into the dependence of photovoltaic performance on interfacial energy alignment in solar cells with mobile ions. *Sol. RRL*, 8(2), 2300742. https://doi.org/10.1002/solr.202300742
- 12. Mortadi, A. et al. (2024). Investigating the influence of absorber layer thickness on the performance of perovskite solar cells: A combined simulation and impedance spectroscopy study. *Mater. Sci. Energy Technol.*, 7, 158–165. https://doi.org/10.1016/j.mset.2023.10.001
- 13. Zhang, N. et al. (2024). Enhancing charge carrier extraction and energy band alignment in perovskite solar cells using interfacial passivation with polar organic molecules. *Chem. Inorganic Mater.*, 2, 100031. https://doi.org/10.1016/j.cinorg.2023.100031
- 14. Denton, A. R. & Ashcroft, N. W. (1991). Vegard's law. *Phys. Rev. A*, 43, 3161–3164. https://doi.org/10.1103/PhysRevA.43.3161
- 15. Burgelman, M. et al. (2000). Modelling polycrystalline semiconductor solar cells. *Thin Solid Films*, 361–362, 527–532. https://doi.org/10.1016/S0040-6090(99)00825-1
- Krishnamoorthy, T. et al. (2015). Lead-free germanium iodide perovskite materials for photovoltaic applications. J. Mater. Chem. A, 47(3), 23829–23832. https://doi.org/ 10.1039/C5TA05741H
- 17. Joshi, T. K. et al. (2020). Computational determination of structural, electronic, optical, thermoelectric and thermodynamic properties of hybrid perovskite CH3CH2NH3GeI3: An emerging material for photovoltaic cell. *Mater. Chem. Phys.*, 251, 123103. https://doi.org/10.1016/j.matchemphys.2020.123103
- 18. Alsalme, A. et al. (2022). Optimization of photovoltaic performance of Pb-free perovskite solar cells via numerical simulation. *Molecules*, 28(1), 224. https://doi.org/10.3390/molecules28010224
- 19. Sabbah, H. (2022). Numerical simulation of 30% efficient lead-free perovskite CsSnGeI<sub>3</sub>-Based Solar Cells. *Mater.*, 15(9), 3229. https://doi.org/10.3390/ma15093229

- 20. Paz Totolhua, E. et al. (2023). Numerical simulation of an inverted perovskite solar cell using a SiOx layer as down-conversion energy material to improve efficiency and stability. *Mater.*, 16(23), 7445. https://doi.org/10.3390/ma16237445
- 21. Li, X. et al. (2024). Stereo-active lone pairs induced giant polarization in a 2D Gebased halide perovskite antiferroelectric. *Adv. Funct. Mater.*, 34(12), 2311944. https://doi.org/10.1002/adfm.202311944
- 22. Stoumpos, C. C. et al. (2015). Hybrid germanium iodide perovskite semiconductors: Active lone pairs, structural distortions, direct and indirect energy gaps, and strong nonlinear optical properties. *J. Am. Chem. Soc.*, 137(21), 6804–6819. https://doi.org/10.1021/jacs.5b01025
- 23. Miah, Md. H. et al. (2024). Band gap tuning of perovskite solar cells for enhancing the efficiency and stability: Issues and prospects. *RSC Adv.*, 14, 15876–15906. https://doi.org/10.1039/D4RA01640H
- 24. Shockley, W. & Queisser, H. J. (1961). Detailed balance limit of efficiency of *p-n* junction solar cells. *J. Appl. Phys.*, 32, 510–519. https://doi.org/10.1063/1.1736034
- 25. Elangovan, N. K. et al. (2024). Recent developments in perovskite materials, fabrication techniques, band gap engineering, and the stability of perovskite solar cells. *Energy Rep.*, 11, 1171–1190. https://doi.org/10.1016/j.egyr.2023.12.068
- 26. Ren, C. et al. (2024). Employing the interpretable ensemble learning approach to predict the bandgaps of the halide perovskites. *Mater.*, 17(11), 2686. https://doi.org/10.3390/ma17112686
- 27. Lei, Y. et al. (2022). Photon energy loss and management in perovskite solar cells. *Energy Rev.*, 1(1), 100003. https://doi.org/10.1016/j.enrev.2022.100003
- 28. Shur, M. (2005). Semiconductors. In Chen, W.-K. (Eds.). *The Electrical Engineering Handbook*. Amsterdam: Academic Press, 153–162. https://doi.org/10.1016/B978 -012170960-0/50015-3
- 29. Siregar, N. et al. (2021). Effect of post-heating temperature on efficiency of dye-sensitized solar cell with ZnO:Al thin films prepared by sol-gel spin coating. *J. Phys. Sci.*, 32(2), 57–70. https://doi.org/10.21315/jps2021.32.2.5
- 30. Saliba, M. et al. (2016). Incorporation of rubidium cations into perovskite solar cells improves photovoltaic performance. *Sci.*, 354(6309), 206–209. https://doi.org/10.1126/science.aah5557
- 31. Hamady, S. O. S. et al. (2019). Development of novel thin film solar cells: Design and numerical optimisation. *J. Phys. Sci.*, 30(Supp.2), 199–205. https://doi.org/10.21315/jps2019.30.s2.17
- 32. Ijaz, S. et al. (2024). A numerical approach to optimize the performance of HTL-free carbon electrode-based perovskite solar cells using organic ETLs. *Heliyon*, 10, e29091. https://doi.org/10.1016/j.heliyon.2024.e29091
- 33. Kavanagh, S. R. et al. (2022). Impact of metastable defect structures on carrier recombination in solar cells. *Faraday Dis.*, 239, 339–356. https://doi.org/10.1039/D2FD00043A
- 34. Zhang, X. *et al.* (2022). High fill factor organic solar cells with increased dielectric constant and molecular packing density. *Joule*, 6(2), 444–457. https://doi.org/10.1016/j.joule.2022.01.006

- 35. Hidayat, R. et al. (2020). Revealing the charge carrier kinetics in perovskite solar cells affected by mesoscopic structures and defect states from simple transient photovoltage measurements. *Sci. Rep.*, 10, 19197. https://doi.org/10.1038/s41598-020-74603-x
- 36. Kopacic, I. et al. (2018). Enhanced performance of germanium halide perovskite solar cells through compositional engineering. *ACS Appl. Energy. Mater.*, 1(2), 343–347. https://doi.org/10.1021/acsaem.8b00007
- 37. Wallace, S. K. et al. (2019). Finding a junction partner for candidate solar cell absorbers enargite and bournonite from electronic band and lattice matching. *J. Appl. Phys.*, 125(5), 055703. https://doi.org/10.1063/1.5079485
- 38. Jan, S. T. & Noman, M. (2023). Comprehensive analysis of heterojunction compatibility of various perovskite solar cells with promising charge transport materials. *Sci. Rep.*, 13, 19015. https://doi.org/10.1038/s41598-023-46482-5
- 39. Pindolia, G. et al. (2022). Optimization of an inorganic lead free RbGeI<sub>3</sub> based perovskite solar cell by SCAPS-1D simulation. *Sol. Energy*, 236, 802–821. https://doi.org/10.1016/j.solener.2022.03.053
- 40. Wang, Y. et al. (2021). Interfacial defect mediated charge carrier trapping and recombination dynamics in TiO<sub>2</sub>-based nanoheterojunctions. *J. Alloys. Compd.*, 872, 159592. https://doi.org/10.1016/j.jallcom.2021.159592
- 41. Noman, M. et al. (2024). Interface engineering and defect passivation for enhanced hole extraction, ion migration, and optimal charge dynamics in both lead-based and lead-free perovskite solar cells. *Sci. Rep.*, 14, 5449. https://doi.org/10.1038/s41598-024-56246-4
- 42. Cheng, N. et al. (2019). A simulation study of valence band offset engineering at the perovskite/Cu<sub>2</sub>ZnSn(Se<sub>1</sub>-xS<sub>x</sub>)<sub>4</sub> interface for enhanced performance. *Mater. Sci. Semicond. Proc.*, 90, 59–64. https://doi.org/10.1016/j.mssp.2018.10.006
- 43. Mavlonov, A. et al. (2024). Influence of valence band offset at the hole transport material/CH<sub>3</sub>NH<sub>3</sub>PbI<sub>3</sub> interface on device performance using fluorinated spiro-OMeTAD. ACS Appl. Energy Mater., 7(14), 5937–5943. https://doi.org/10.1021/acsaem.4c01189
- 44. Bichave, S. et al. (2023). Analysis of varying ETL/HTL material for an effective perovskite solar cell by numerical simulation. *Mater. Today Proc.* https://doi.org/10.1016/j.matpr.2023.01.190
- 45. Hossain, M. K. et al. (2023). An extensive study on multiple ETL and HTL layers to design and simulation of high-performance lead-free CsSnCl<sub>3</sub>-based perovskite solar cells. *Sci. Rep.*, 13, 2521. https://doi.org/10.1038/s41598-023-28506-2